Journal of Inorganic Biochemistry 218 (2021) 111404

Contents lists available at ScienceDirect

Journal of Inorganic Biochemistry

journal homepage: www.elsevier.com/locate/jinorgbio

Ru complexes containing Cp, mPTA and natural purine bases (mPTA = methyl-N-1,3,5-triaza-7-phosphaadamantane): Evaluation of their antiproliferative activity, solubility and redox properties

Lazhar Hajji, Cristobal Saraiba-Bello, Franco Scalambra, Gaspar Segovia-Torrente, Antonio Romerosa *

Área de Química Inorgánica-CIESOL, Facultad de Ciencias Experimentales, Universidad de Almería, 04071 Almería, Spain

ARTICLE INFO

Keywords:
Antiproliferative activity
Ruthenium
Water-soluble complexes
mPTA
Natural purines

ABSTRACT

Complexes [RuCp(Adeninate–κ*N9*)(mPTA)$_2$](Cl$_{0.5}$)(CF$_3$SO$_3$)$_{2.5}$·H$_2$O (**1·H$_2$O**), [RuCp(Guaninate-κ*N7*)(mPTA)$_2$](CF$_3$SO$_3$)$_2$·H$_2$O (**2·H$_2$O**), [RuCp(Theophyllinate-κ*N7*)(mPTA)$_2$](CF$_3$SO$_3$)$_2$·1.5H$_2$O (**3·1.5H$_2$O**) and [RuCp(Pur-κ*N*)(mPTA)(PPh$_3$)](CF$_3$SO$_3$) (**4–6**) (Pur = Adeninate, Guaninate, Teophyllinate; mPTA = *N*-methyl −1,3,5-triaza-7-phosphaadamantane) have been synthesized and characterized. Structure of complexes 1·H$_2$O and 3·1.5H$_2$O were determined by single-crystal X-ray diffraction. Solubility in water, Log *P*, electrochemical properties and antiproliferative activities of the complexes (against cisplatin-sensitive T2 and cisplatin-resistant SKOV3 cell lines) have been assessed and discussed.

1. Introduction

From the sixties, when Rosenberg discovered the anticancer properties of the [PtCl$_2$(NH$_3$)$_2$] (cisplatin) [1], platinum complexes are widely investigated as a chemotherapeutic agent [2]. However, despite the great advances in the understanding of the action mechanism of Pt complexes that have provided valuable information for the synthesis of new more effective against cancer complexes, they are accompanied by serious drawbacks like high toxicity and drug resistance [3,4]. The proposed alternatives explore the use of complexes with different metals to platinum [5]. A valuable alternative is Ru-compounds: Ru has a ligand exchange kinetic similar to platinum(II), more available oxidation states (II, III, IV) than Pt, the ability to "mimic" the iron in a wide variety of biological molecules and additionally, is less toxic than iron and Pt [6–8].

We have been involved in the synthesis of water-soluble platinum [9,10] and ruthenium [11] complexes containing the phosphine PTA and its derivative mPTA (PTA = 1,3,5-triaza-7-phosphaadamantane; mPTA = *N*-methyl-1,3,5-triaza-7-phosphaadamantane) with purines and thiopurines that showed interesting antiproliferative activity on *cis*platin-sensitive T2 and *cis*platin-resistant SKOV3 cell lines [12].

Our last paper about this subject [13] showed as among the complexes containing natural purines of general formula [RuCp(Pur-κ*N*)(PTA)$_2$) and [RuCp(Pur-κ*N*)(PTA)(PPh$_3$)] (Pur = Adenine, Guanine, Theophylline) only [RuCp(Adeninate–κ*N7*)(PPh$_3$)(PTA)] showed cytotoxicity similar to cisplatin on T2 cell line and better profile on SKOV3 cell line. This behaviour was proposed to be favoured by the appropriate hydro−/lipophilic balance (Log *P* = 1.4) reached upon coordination to the ruthenium of one hydrophilic PTA and one lipophilic PPh$_3$. Nevertheless, another possibility that was proposed to justify the antiproliferative activity of [RuCp(Adeninate–κ*N7*)(PPh$_3$)(PTA)] is its probable interaction by hydrogen bonds with the DNA-adenines, such as observed in its crystal structure. To obtain more information about possible factors determining the antiproliferative activity of these complexes, the analogues [RuCp(Pur-κ*N*)(mPTA)$_2$)(CF$_3$SO$_3$)$_2$ (**1**–**3**) and [RuCp(Pur-κ*N*)(mPTA)(PPh$_3$)(CF$_3$SO$_3$) (**4**–**6**) (Pur = Adenine, Guanine, Theophylline), which contain the cationic methylated-PTA ligand (mPTA), were synthesized and their antiproliferative activity assessed against the tumoral cell lines T2 and SKOV3. The phosphine mPTA displays similar basicity to PTA but it is positively charged and this fact made it significantly more soluble in water and practically insoluble in organic solvents, which will change the solubility properties of the complexes but also probably how this complex could interact with the DNA.

* Corresponding author.
E-mail address: romerosa@ual.es (A. Romerosa).

https://doi.org/10.1016/j.jinorgbio.2021.111404
Received 31 December 2020; Received in revised form 16 February 2021; Accepted 16 February 2021
Available online 23 February 2021

2. Experimental

2.1. General procedures

All chemicals were reagent grade and were used as received by commercial suppliers unless otherwise stated. The solvents were all degassed and distilled according to standard procedures [13]. All reactions and manipulations were routinely performed under a dry nitrogen atmosphere by using standard Schlenk-tube techniques. The ligand mPTA and starting complexes $[RuClCp(mPTA)_2](CF_3SO_3)_2$ and $[RuClCp(PPh_3)(mPTA)](CF_3SO_3)$ were prepared as described in the literature [11]. Solvents for NMR measurements (Cortec-Euriso-top) were dried over molecular sieves (4 Å). ^1H, $^{31}P\{^1H\}$ NMR and $^{13}C\{^1H\}$ NMR spectra were recorded on a Bruker DRX300 spectrometer operating at 300.13 MHz (^1H), 121.49 MHz (^{31}P) and 75.47 MHz (^{13}C), respectively. Peak positions are relative to tetramethylsilane and were calibrated against the residual solvent resonance (^1H) or the deuterated solvent multiplet (^{13}C). Chemical shifts for $^{31}P\{^1H\}$ NMR were measured relative to external 85% H_3PO_4 with downfield values taken as positive. Infrared spectra were recorded on KBr discs using an FT-IR ATI Mattson Infinity Series. Elemental analysis (C, H, N, S) was performed on a Fisons Instruments EA 1108 elemental analyser. The solubility in water of the synthesized complexes was determined by UV–vis spectrophotometry techniques. Chlorine was determined by volumetric titration with the method of Volhard after the oxidative break-up of the sample [14].

2.2. Synthesis of $[RuCp(Ad\text{-}\kappa N9)(mPTA)_2](Cl_{0.5})(CF_3SO_3)_{2.5}\cdot H_2O$ (1·H₂O)

Adenine (0.164 g, 0.122 mmol) and the complex $[RuCpCl(mPTA)_2](CF_3SO_3)_2$ (0.086 g, 0.102 mmol) were added into 10 mL of H_2O and the mixture stirred for 15 min at room temperature and kept to reflux for 4 h. The resulting dissolution was cooled at room temperature and the solvent reduced to 1 mL. Slow evaporation of the resulting dissolution provided yellow crystals useful for single crystal X-ray determination, which were filtered and air-dried.

Yield crystals: 0.084 g, 58%. $S_{25,H2O}(mg/cm^3)$: 25.9. Elemental analysis for $C_{26.5}H_{41}Cl_{0.5}F_{7.5}N_{11}O_8P_2Ru_1S_{2.5}$ (1045.07): Found C, 30.12; H, 4.17; N, 14.34; S, 7.25%; Cl, 1.65%; calcd. C, 30.46; H, 3.95; N, 14.74; S, 7.67%; Cl, 1.70%. IR (KBr, cm^{-1}): ν(OH + NH) 2500–3600 (mws); ν(NH) 3419 (s); ν(CH) 2796, 2980 (m); $\delta(NH_2)$ 1632, 1602 (s); ν(C=C + C=N) 1547 (m); ν_{mPTA}(CH) 1459, 1418 (m); ν(SO) 1256 (m); ν(NC) 1029 (s). ^1H NMR (293 K, D_2O): δ 2.83 (s, CH_3N_{mPTA}, 6H); 3.94–4.20 (m, CH_2P_{mPTA}, 12H); 4.36–4.61 (m, CH_2N_{mPTA}, 12H); 5.02 (s, Cp, 5H); 7.70 (s, C2-H_{Ad}, 1H); 8.30 (s, C8-H_{Ad}, 1H). $^{13}C\{^1H\}$ NMR (293 K, D_2O): δ 49.45 (s, CH_3N_{mPTA}); 53.39 (d, $^1J_{CP}$ = 64.08 Hz, NCH_2P_{mPTA}); 61.81 (s, $CH_3NCH_2P_{mPTA}$); 69.10 (s, NCH_2N_{mPTA}); 80.14 (s, $CH_3NCH_2N_{mPTA}$); 80.37 (s, Cp); 118.95 (s, C5); 143.21 (s, C8); 150.18 (s, C4); 152.16 (s, C2); 156.68 (s, C6). $^{31}P\{^1H\}$ NMR (293 K, D_2O): δ − 10.02 (s, mPTA). E_a(mV) = 861 [Ru(III)/Ru(II)]; E_c (mV) = 776; $E_{½}$ (mV) = 818.5; ΔE (mV) = 85. Log *P* = 0.047.

2.3. Synthesis of $[RuCp(Gu\text{-}\kappa N9)(mPTA)_2](CF_3SO_3)_2\cdot H_2O$ (2·H₂O)

Guanine (0.017 g, 0.113 mmol) and KOH (0.063 g, 0.122 mmol) were added into 10 mL of H_2O. After 15 min the complex $[RuCpCl(mPTA)_2](CF_3SO_3)_2$ (0.086 g, 0.102 mmol) was joined. The mixture was refluxed for 2 h, cooled at room temperature and the solvent reduced to dryness, 5 mL of EtOH added and the mixture sonicated for 30 min at 50 °C. The yellow powder was filtered and dried under vacuum.

Yield: 0.067 g, 64%. $S_{25,H2O}(mg/cm^3)$: 9.2. Elemental analysis for $C_{26}H_{43}F_6N_{11}O_9P_2RuS_2$ (995.11 g.mol^{-1}): Found C, 30.98; H, 4.47; N, 15.32; S, 6.42%; calcd. C, 31.39; H, 4.36; N, 15.49; S, 6.45%. IR (KBr, cm^{-1}): ν(NH) 3445 (m); $\delta(NH_2)$ 1660 (s); ν(C6 = O) 1632 (s); ν(C=C + C=N) 1601 (m); ν_{mPTA}(CH) 1456, 1416 (m); ν_{mPTA}(CN) 1224, 1287 (m); ν(SO) 1028(f), 1252 (s); ν_{Gu} (NC) 972 (s). ^1H NMR (293 K, D_2O): δ 2.75 (s, CH_3N_{mPTA}, 6H); 3.87–4.14 (m, CH_2P_{mPTA}, 12H); 4.24–4.53 (m, CH_2N_{mPTA}, 12H); 4.91 (s, Cp, 5H); 7.27 (s, C8H, 1H). $^{13}C\{^1H\}$ NMR (293 K, D_2O): δ 49.11 (s, CH_3N_{mPTA}); 53.17 (d, $^1J_{CP}$ = 55.53 Hz, NCH_2P_{mPTA}); 61.26 (s, $CH_3NCH_2P_{mPTA}$); 68.79 (s, NCH_2N_{mPTA}); 79.18 (s, $CH_3NCH_2N_{mPTA}$); 79.97 (s, Cp); 119.54 (s, C5); 121.65 (q, $^1J_{CF}$ = 316.86 Hz, OSO_2CF_3); 140.22 (s, C8); 153.45 (s, C4); 153.89 (s, C2); 162.45 (s, C6). $^{31}P\{^1H\}$ NMR (293 K, D_2O): δ − 9.91 (s, mPTA). E_a(mV) = 712 [Ru(III)/Ru(II)]; E_c (mV) = 625; $E_{½}$ (mV) = 668.5; ΔE (mV) = 87. Log *P* = − 0.38.

2.4. Synthesis of $[RuCp(Tf\text{-}\kappa N7)(mPTA)_2](CF_3SO_3)_2\cdot 1.5\ H_2O$ (3·1.5H₂O)

Using a similar synthetic procedure to that for 2, theophylline (0.023 g, 0.130 mmol) was added into 10 mL of aqueous KOH solution (0.0103 M), stirred for 15 min, and then $[RuClCp(mPTA)_2](CF_3SO_3)_2$ (0.105 g, 0.125 mmol) was added. The product was obtained as a yellow powder. Crystals of this complex were obtained by recrystallization in H_2O.

Yield: 0.32 g, 45%. $S_{25,H2O}(mg/cm^3)$: 16.1. Elemental analysis for $C_{28}H_{45}F_6N_{10}O_{9.5}P_2RuS_2$ (1015.12): Found C, 32.87; H, 4.57; N, 13.42; S, 5.91%; calcd. C, 33.14; H, 4.47; N, 13.80; S, 6.17%. IR (KBr, cm^{-1}): $\nu(CH_3)$ 3119 (m); δ(CH) 2956 (m); δ(C6 = 0) 1692 (s); δ(C2 = O) 1649 (s); ν(C=C + C=N) 1530 (s); ν(S=O) 1029 (s), 1251 (s). ^1H NMR (293 K, D_2O): δ 2.84 (s, CH_3N_{mPTA}, 6H); 3.29 (s, CH_3N1, 3H); 3.40 (s, CH_3N3, 3H); 3.91–4.07 (m, CH_2P_{mPTA}, 12H); 4.33–4.45 (m, CH_2N_{mPTA}, 12H); 4.86 (s, Cp, 5H); 7.65 (s, C8H, 1H). $^{13}C\{^1H\}$ NMR (293 K, D_2O): δ 28.01 (s, CH_3N1); 30.19 (s, CH_3N3); 49.11 (s, CH_3N_{mPTA}); 52.56 (d, $^1J_{CP}$ = 62.11 Hz, NCH_2P_{mPTA}); 60.36 (s, $CH_3NCH_2P_{mPTA}$); 68.83 (s, NCH_2N_{mPTA}); 80.05 (s, $CH_3NCH_2N_{mPTA}$); 80.54 (s, Cp); 110.53 (s, C5); 119.53 (q, $^1J_{CF}$ = 317.89 Hz, OSO_2CF_3); 148.56 (s, C8); 152.56 (s, C4); 154.50 (s, C2); 157.30 (s, C6). $^{31}P\{^1H\}$ NMR (293 K, D_2O): δ − 9.67 (s, mPTA). E_a(mV) = 737 [Ru(II)/Ru(III)]; E_c (mV) = 639; $E_{½}$ (mV) = 688; ΔE = 49. Log *P* = −0.69.

2.5. Synthesis of $[RuCp(Ad\text{-}\kappa N9)(PPh_3)(mPTA)](CF_3SO_3)$ (4)

Adenine (0.021 g, 0.16 mmol) and KOH (0.010 g, 0.17 mmol) were introduced into 10 mL of EtOH and the resulting mixture stirred at room temperature for 15 min. Then, the complex $[RuCpCl(PPh_3)(mPTA)](CF_3SO_3)$ (0.101 mg, 0.13 mmol) was also added and after 10 min stirring at room temperature the mixture was kept at reflux for 4 h. The obtained solution was cooled, filtered and concentrated to 2 mL, followed by the addition of 5 mL of Et_2O. The yellow precipitate obtained was filtered, washed with Et_2O (2 × 2 mL) and dried under vacuum.

Yield: 106.50 mg, 87%. $S_{25,H2O}(mg/cm^3)$: 1.3. Elemental analysis for $C_{36}H_{39}F_3N_8O_3P_2RuS$ (884.13 g.mol^{-1}), Found C, 48.77; H 4.63; N 12.26; S 3.31%; calcd. C, 48.92; H, 4.45; N, 12.68; S, 3.63%. IR (KBr, cm^{-1}): ν(OH + NH) 2500–3600 (mws); $\nu(NH_2)$ 1623, 1604 (s); ν(C=C + C=N) 1541 (m); ν(SO) 1228, 1030 (s); ^1H NMR (20 °C, $CDCl_3$): δ 2.80 (bs, CH_3N_{mPTA}, 3H); 3.39–3.75 (m, CH_2P_{mPTA}, 6H); 4.22–4.58 (m, CH_2N_{mPTA}, 6H); 4.74 (s, Cp, 5H); 7.16–7.55 (m, aromatics, 15H); 8.28 (s, C8H, 1H). $^{13}C\{^1H\}$ NMR (20 °C, $CDCl_3$): δ 49.17 (s, CH_3N_{mPTA}); 51.10 (d, $^1J_{CP}$ = 12.28 Hz, NCH_2P_{mPTA}); 52.76 (d, $^1J_{CP}$ = 13.8 Hz, $CH_3NCH_2P_{mPTA}$); 62.04 (s, $CH_3NCH_2N_{mPTA}$); 69.19 (s, NCH_2N_{mPTA}); 81.20 (s, Cp); 122.33–137.20 (m, aromatics); 118.41 (s, C5); 148.47 (s, C8); 149.51 (s, C4); 154.47 (d, C2); 161.57 (s, C6). $^{31}P\{^1H\}$ NMR (20 °C, $CDCl_3$): δ − 14.34 (d, $^1J_{PP}$ = 40.58 Hz); 50.70 (d, $^1J_{PP}$ = 40.58 Hz). E_a(mV) = E_{ox1} = 730 [Ru(II)/Ru(III)]; E_{ox2} = 837 [Ru(III)/Ru(IV)]. Log *P* = 0.4.

2.6. Synthesis of $[RuCp(Gu\text{-}\kappa N9)(PPh_3)(mPTA)](CF_3SO_3)$ (5)

The yellow complex 5 was obtained by the procedure described above for 4 but using guanine (0.024 g, 0.16 mmol).

Yield: 51.0 mg, 82%. $S_{25,H2O}(mg/cm^3)$: 1.4. Elemental analysis for $C_{36}H_{39}F_3N_8O_4P_2RuS$ (884.13 g.mol^{-1}), Found C, 48.75; H 4.60; N

12.32; S 3.33%; calcd. C, 48.92; H, 4.45; N, 12.68; S, 3.63%. IR (KBr, cm^{-1}): ν(OH + NH) 2400–3600 (mws); ν(NH_2) 1660 (s); ν(C=O) 1623 (s); ν(C=C + C=N) 1601 (s); ν(SO) 1257 (s). ^{1}H NMR (20 °C, DMSO-d_6): δ 2.74 (s, CH_3N_{mPTA}, 3H); 3.87–4.14 (m, CH_2P_{mPTA}, 6H); 4.15–4.82 (m, CH_2N_{mPTA}, 6H); 4.82 (s, Cp, 5H); 7.10–7.70 (m, aromatics, 15H). ^{13}C{^{1}H} NMR (20 °C, DMSO-d_6): δ 49.18 (s, CH_3N_{mPTA}); 53.12 (d,$^1J_{CP}$ = 15.52 Hz, NCH_2P_{mPTA}); 61.24 (s, $CH_3NCH_2P_{mPTA}$); 68.60 (s, $CH_3NCH_2N_{mPTA}$); 79.52 (s, NCH_2N_{mPTA}); 81.37 (s, Cp); 119.55 (q,$^1J_{CF}$ = 316.52 Hz, OSO_2CF_3); 118.73 (s, C5); 128.28–134.55 (m, aromatics); 150.82 (s, C8); 151.50 (s, C4); 158.05 (s, C2); 162.60 (s, C6). ^{31}P{^{1}H} NMR (20 °C, DMSO-d_6): δ 52.35 (d,$^2J_{PP}$ = 41.28 Hz); −15.38 (d,$^2J_{PP}$ = 41.28 Hz). E_a(mV) = 796 [Ru(II)/Ru(III)]. Log *P* = 0.35.

2.7. Synthesis of [RuCp(Tf-κN7)(PPh3)(mPTA)](CF3SO3) (6)

The complex 6 was obtained as a yellow powder by the procedure described above for 4 but using theophylline (0.029 mg, 0.16 mmol).

Yield: 38.0 mg, 75%. $S_{25,H2O}$(mg/cm^3): 1.7. Elemental analysis for $C_{38}H_{42}F_3N_7O_5P_2RuS$ (929.14 g.mol^{-1}), Found C, 48.85; H 4.78; N 10.24; S 3.12%; calcd. C, 49.14; H, 4.56; N, 10.56; S, 3.45%. IR (KBr, cm^{-1}): ν(C2 = O) 1682 (s); ν(C6 = O) 1628 (s); ν(C=C + C=N) 1526 (s); ν(SO) 1256 (s). ^{1}H NMR (20 °C, DMSO-d_6): δ 2.66 (s, CH_3N_{mPTA}, 3H); 3.18 (s, N1-CH_3, 3H); 3.30 (s, N3-CH_3, 3H); 3.70–3.92 (m, NCH_2N_{mPTA}, 6H); 4.15–4.31 (m, NCH_2P_{mPTA}, 6H); 4.78 (s, Cp, 5H); 6.72 (s, C8H, 1H); 7.08–7.74 (m, aromatic, 15H). ^{13}C{^{1}H} NMR (20 °C, DMSO-d_6): δ 28.40 (s, CH_3N1); 29.82 (s, CH_3N3); 49.58 (s, CH_3N_{mPTA}); 49.91 (d,$^1J_{CP}$ = 12.55, NCH_2P_{mPTA}); 51.42 (d,$^1J_{CP}$ = 15.23 Hz, $CH_3NCH_2P_{mPTA}$); 60.04 (s, $CH_3NCH_2N_{mPTA}$); 68.75 (s, NCH_2N_{mPTA}); 81.60 (s, Cp); 128.53–133.90 (m, aromatics); 116.75 (s, C5); 146.37 (s, C8); 151.54 (s, C4); 154.60 (s, C2); 157.41 (s, C6). ^{31}P{^{1}H} NMR (20 °C, DMSO-d_6): δ −16.87 (d,$^2J_{PP}$ = 43.23 Hz, P_{mPTA}); 51.02 (d,$^2J_{PP}$ = 43.23 Hz, P_{PPh3}). E_a(mV) = 710 [Ru(II)/Ru(III)]. Log *P* = 0.23.

2.8. X-ray structure determinations

Data of compounds **1·H2O** and **3·1.5H2O** were collected on a Bruker APEX CCD diffractometer using graphite monochromated Mo Kα radiation (λ = 0.7107 Å) at 273.15 K. The crystal parameters and other experimental details of the data collections are summarized in Table 1. Using Olex2 [15], the structure was solved with the XT structure solution program [16], using Intrinsic Phasing and refined anisotropically with the SHELXL refinement package [17], using Least Squares minimisation. All hydrogen atoms were included in calculated positions and refined using a riding model.

2.9. Growth inhibition assays

Cell growth inhibition assays were carried out using the *cis*platin-sensitive T2 human cell line and the *cis*platin-resistant SKOV3 cell line. T2 is a cell hybrid obtained by the fusion of the human lymphoblastoid line 174 (B lymphocyte transformed by the Epstein-Barr virus) with the CEM human cancer line (leukaemia T) while SKOV3 is derived from a human ovarian tumour. The cells were seeded in triplicate in 96-well trays at a density of $50{\cdot}10^3$ in 50 μL of AIM-V medium for T2, $25{\cdot}10^3$ in 50 μL of AIM-V™ medium for SKOV3. Stock solutions (10 mM) of the Ruthenium complexes **1**–**6** were prepared in DMSO and diluted in AIM-V medium to give a final concentration of 2, 10 and 50 μM. Cisplatin was employed as a control for the cisplatin-sensitive T2 cell line and the cisplatin-resistant SKOV3. Untreated cells were placed in every plate as a negative control. The cells were exposed to the compounds for 72 h and then 25 μL of a 4,5-dimethylthiozol-2-yl)2,5-diphenyltetrazolium bromide solution (12 mM) were added. After two hours of incubation, 100 μL of lysing buffer (50% DMF + 20% SDS, pH 4.7) were added to convert 4,5-dimethylthiazol-2-yl-2,5-diphenyltetrazolium bromide into a brown coloured formazan. After additional 18 h the solution absorbance, proportional to the number of live cells, was measured by spectrophotometer and converted in % of growth inhibition [18].

Table 1
Crystallographic data for **1·H2O** and **3·1.5H2O**.

	1·H2O	**3·1.5H2O**
CCDC number	2,043,488	2,043,489
Empirical formula	$C_{53}H_{86}F_{15}N_{22}O_{18}P_4Ru_2S_5$	$C_{56}H_{90}F_{12}N_{20}O_{19}P_4Ru_2S_4$
Formula weight	2090.75	2029.73
Temperature [K]	273.15	273.15
Crystal system	triclinic	triclinic
Space group	P-1	P-1
a [Å]	11.7996(3)	10.1364(8)
b [Å]	11.9041(3)	12.2966(10)
c [Å]	16.6699(5)	15.9761(13)
α [°]	76.0500(10)	93.567(2)
β [°]	70.7750(10)	100.2560(10)
γ [°]	64.6750(10)	90.0380(10)
Volume [$Å^3$]	1984.63(9)	1955.6(3)
Z	1	1
ρ_{calc} [g/cm^3]	1.749	1.724
M [mm^{-1}]	0.707	0.684
F(000)	1065.0	1038.0
Radiation	MoKα (λ = 0.71073)	MoKα (λ = 0.71073)
2Θ range [°]	4.224 to 54.206	5.192 to 46.302
Index ranges	$-14 \le h \le 15$, $-14 \le k \le 15$, $-21 \le l \le 17$	$-10 \le h \le 11$, $-13 \le k \le 13$, $-17 \le l \le 15$
Reflections collected	13,789	9260
Independent reflections	8549 [R_{int} = 0.0298, R_{sigma} = 0.0610]	5483 [R_{int} = 0.0532, R_{sigma} = 0.1034]
Data/restraints/parameters	8549/575/624	5483/632/574
Goodness-of-fit on F^2	1.019	1.022
Final R indexes [$I \geq 2\sigma$ (I)]	R_1 = 0.0448, wR_2 = 0.1130	R_1 = 0.0725, wR_2 = 0.1780
Final R indexes [all data]	R_1 = 0.0587, wR_2 = 0.1223	R_1 = 0.1041, wR_2 = 0.2017

2.10. Stability tests of the complexes against O_2 and H_2O

Complexes are stable for months in the solid-state under air. In water and ethanol solution they are stable for more than 2 days under air and more than a week under an inert atmosphere of Ar. The assessment of the stability under air was performed dissolving 0.01 g of the complex in 0.5 mL of D_2O into a 5 mm NMR tube. The solution was cooled to 5 °C and then the air was bubbled throughout it for 5 min. ^{31}P{^{1}H} NMR showed that slow but significant decomposition of the complexes starts after 2 days at 40 °C. Reactivity against DMSO was tested dissolving the complexes in 0.1 mL of DMSO-d_6 and just after dissolution adding 0.4 mL of D_2O. Checking by ^{31}P NMR at time intervals showed that the complexes were stable more than 2 days at 40 °C.

2.11. Cyclic voltammetry experiments

A standard disposition for the voltammetry measurements was used including a three-electrode glass cell consisting of a platinum disk working electrode, a platinum wire auxiliary electrode and a metallic Ag reference electrode, which were connected to a VersaSTAT3 apparatus. The absence of electro-active impurities in the supporting electrolyte ($LiClO_4$, 0.05 M) was previously determined over the solvent window and a similar concentration of the analyte (0.1 mM) in DMF was employed in all the measurements. All the signals are referenced to the Ag/AgCl electrode.

2.12. Octanol-water partition coefficient determination

The experiments to calculate the complex partition coefficient (Log *P*) were performed in octanol/water by the slow-stirring method

[19–21], which was tailored to the solubility of the complexes. Complexes were dissolved in octanol previously saturated with distilled water in a concentration range from 10^{-4} to 10^{-3} M. Into a flask with a stirring bar, water (10 mL) previously saturated with octanol was added. Then, stable solutions of octanol (10 mL) were added with a syringe, avoiding the formation for emulsions. The flask was closed and the contents stirred slowly at 25 ± 1 °C. Periodically, samples were taken from the octanol and water phases with a syringe until the concentrations in both phases, measured by UV–vis spectroscopy, stabilized. Although the stability of the complexes did not require an inert atmosphere, the experiments were performed under N_2 as a precaution.

3. Results and discussions

3.1. Synthesis and characterization of the complexes

Reactivity of starting complexes $[RuCpCl(mPTA)_2](CF_3SO_3)_2$ and $[RuCpCl(PPh_3)(mPTA)](CF_3SO_3)_2$ was initially checked with non-deprotonated purines to determine their ability to react with the complexes, which provide us how easy could be the substitution of one of the ligands bonded to the metal by a purine base. A mixture of products was obtained in all the cases despite the numerous attempts made with different reaction conditions and solvents, except the reaction of $[RuCpCl(mPTA)_2](CF_3SO_3)_2$ with adenine, which gave a pure product that was isolated as crystals (**1·H$_2$O**) adequate for single-crystal X-ray diffraction (Scheme 1). The IR spectrum of the complex shows a wide absorption band due to ν(OH + NH) from 2500 cm^{-1} to 3600 cm^{-1}, quite similar to that found in the free adenine, suggesting that the N7 is protonated and the complex is involved in a hydrogen bond network through the N atoms of the adenine ligand. The band at 1256 cm^{-1} ascribable to the ν(SO) supported the presence of the triflate in the composition of the complex. The $^{31}P\{^1H\}$ NMR is characterized by a unique signal at −10.02 ppm, which match well with the phosphorous of the mPTA. The ^1H NMR spectrum agrees with the proposed composition for the complex. The most significant signals are a singlet at 5.02 ppm that only can be ascribable to one Cp and at 7.70 ppm and 8.30 ppm the signals due to adenine-H2 and -H8. The cyclic voltammogram of the complex showed reversible oxidation of a single electron with $E_{1/2}$ = 818.5 mV (ΔV = 85), which is due to the Ru(II)/Ru(III) couple. The proposed composition of the complex was finally supported by the resolution of its crystal structure by single-crystal X-ray diffraction, which will be discussed later.

The other complexes obtained in this work were synthesized by the previous deprotonation of the purine with KOH and further reaction with the starting complex. For what concern $[RuCp(Gu\text{-}\kappa N9)(mPTA)_2](CF_3SO_3)_2$ (**2**), it was synthesized and isolated by the reaction in the water of $[RuCpCl(mPTA)_2](CF_3SO_3)_2$ with K[guanidinate] previously obtained by reaction of guanidine and KOH. The elemental analysis, IR and NMR spectra support the proposed composition for the complex. For **2** the singlet observed at 7.27 ppm in ^1H NMR is characteristic for the C8H of the guanidine. The $^{31}P\{^1H\}$ NMR spectrum displays a singlet at −9.91 ppm, at the somewhat lower field than in complex **1**. For **2** the cyclic voltammogram shows a reversible 1-electron-oxidation with $E_{1/2}$ = 668.5 mV (ΔV = 43.5).

Finally, the yellow derivative containing theophylline $[RuCp(Tf\text{-}\kappa N7)(mPTA)_2](CF_3SO_3)_2{\cdot}1.5H_2O$ (**3·1.5H$_2$O**) was obtained by the same procedure employed with **2** but in this case, single crystals were obtained from a water solution. The purity of the complex was determined by a unique singlet at −9.67 ppm in the $^{31}P\{^1H\}$ NMR spectrum due to the P_{mPTA}, which arises almost at the same chemical shift than for **2**. The cyclic voltammogram of **3** showed a reversible oxidation wave corresponding to a single electron. The anodic signal, corresponding to the oxidation pair appeared at E_a = 737 mV due to Ru(II)/Ru(III) and the cathodic signal at E_c = 639 mV, being the half-wave potential of 688 mV.

Complex **4**–**6** containing one mPTA and one PPh_3, were obtained by reaction of the adenine, guanine or theophylline respectively, with KOH and $[RuClCp(PPh_3)(mPTA)]$ in refluxing EtOH (Scheme 2) as the starting complex is not soluble enough in the water.

The elemental analysis of $[RuCp(Ad\text{-}\kappa N9)(mPTA)(PPh_3)](CF_3SO_3)$ (**4**) agrees with the proposed composition but also the IR spectrum shows the expected bands for the proposed composition. It is important to point out that the IR spectrum displays a large wide absorption ν(OH + NH) band from 2500 cm^{-1} to 3600 cm^{-1}, which is similar, but not the same, to that found in the free adenine and complex **1**. These pieces of evidence suggest that the complex is involved in an extended hydrogen bond network but also that adenine is coordinated by N9 but being the N7 deprotonated. The ^1H NMR of **4** displays similar signals to those for **1**, except for those corresponding to the PPh_3 ligand that overlaps with the resonance of adenine-H2. The chemical shift of the Cp (4.74 ppm) arises at the higher field than in **1** (5.02 ppm). The $^{31}P\{^1H\}$ NMR display two doublets: one at −14.34 ppm, at chemical shift similar to that found for mPTA in **1**, and another at 50.70 ppm that is due to the PPh_3. The redox behaviour for this complex studied by cyclic voltammetry is characterized by two irreversible oxidation waves at 730 mV and 837 mV due to the oxidation processes Ru(II)/Ru(III) and Ru(III)/Ru(IV).

The synthesis of the complex **5**, which contain guanine, was accomplished by a similar procedure to that used for the synthesis of complex **4**. The IR spectrum of **5** showed, in contrast to **2**, a manifold of wide bands from 2400 cm^{-1} to 3600 cm^{-1}, supporting the presence of guanidine in the complex and suggesting that it is involved in an extended hydrogen-bonding network. The $^{31}P\{^1H\}$ NMR display two doublets at −15.38 ppm and 52.35 ppm, assigned to mPTA and PPh_3 respectively. It is important to point out that in the ^1H NMR the resonance corresponding to Guanine-H8 is hidden under the aromatic signals but the rest of the expected signals arise at the similar chemical shift to complex **2**. The most significant difference between the $^{13}C\{^1H\}$ NMR of this complex and the guanine complex **2**, are the aromatic signals due

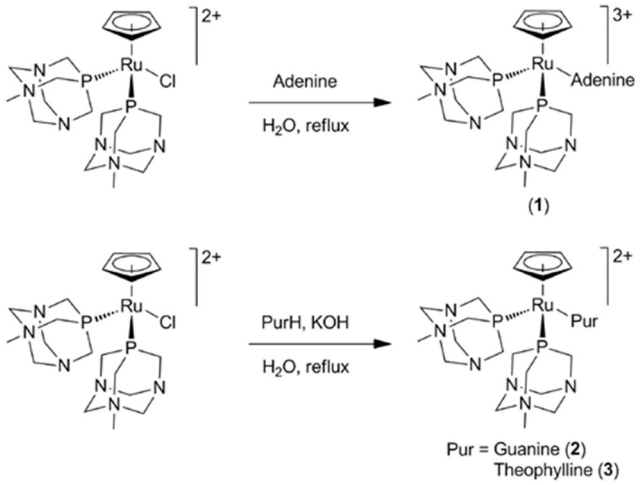

Scheme 1. Synthesis of **1**–**3**.

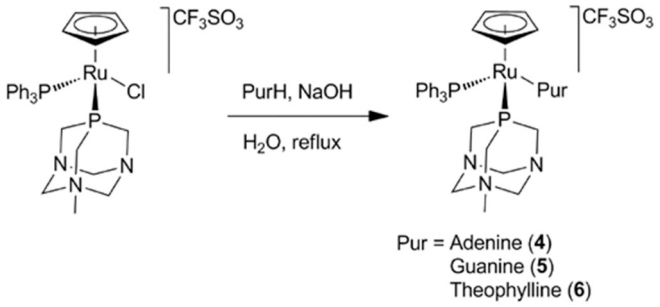

Scheme 2. Synthesis of **4**–**6**.

to the PPh_3. The cyclic voltammogram of this complex shows a unique oxidation process at 796 mV corresponding at Ru(II)/Ru(III).

Finally, the complex **6** containing theophylline, mPTA and PPh_3 was prepared by the same procedure used for complexes **4** and **5**. The IR is similar to that for complex **3** and therefore, it agrees with the presence of the theophylline and mPTA in the complex as well as with the deprotonation of the purine-N7 atom, suggesting that the purine is coordinated to the metal by this atom. The spectroscopic properties agree well with the proposed composition for this complex. Finally, a unique oxidation wave is observed at 710 mV in the cyclic voltammogram due to Ru(II)/Ru(III).

*3.2. Crystal structure of [RuCp(Adenine–κN9)(mPTA)$_2$](Cl)$_{0.5}$(CF$_3$SO$_3$)$_{2.5}$·H$_2$O (**1·H$_2$O**) and [RuCp(Tf-κN7)(mPTA)$_2$](CF$_3$SO$_3$)$_2$·1.5H$_2$O (**3·1.5H$_2$O**)*

Yellow single crystals of compound **1·H$_2$O** were obtained by evaporation of a concentrated solution of the complex in H_2O. The asymmetric unit cell contains one molecule of $[RuCp(Ad\text{-}\kappa N9)(mPTA)_2]^{3+}$, one disordered water molecule, half disordered Cl^- and 2.5 triflate anions, being one of them disordered. The most relevant bond distances and angles are reported in Table 2.

The molecular structure of the complex (Fig. 1) consists of a ruthenium atom coordinated in a distorted octahedral geometry to a Cp, two mPTA, and a molecule of adenine through its nitrogen atom N9. As observed for the parent compound $[RuClCp(mPTA)_2](CF_3SO_3)_2$, Ru—P bond lengths and P-Ru-P angles are elongated concerning analogue complexes containing two neutral PTA ligands. The Ru-$Cp_{centroid}$ distance is slightly larger than in $[RuClCp(mPTA)_2](CF_3SO_3)_2$, while the Ru—N bond length is similar to $[RuCp(Ad\text{-}\kappa N9)(PTA)_2]$ (Ru-$Cp_{centroid}$ = 1.857 Å; Ru-P1 = 2.2725(9) Å; Ru-P2 = 2.2582(9) Å; Ru-N1 = 2.117(3) Å) [22], The P-C and C-N distances and angles in the mPTA ligands are found in the range of similar complexes [23].

The complex molecules are found to be dimerized about an inversion point by hydrogen bonds involving the adenine nitrogen atoms N1 and N10 (Fig. 2). This behaviour was observed also in the complex $[RuCp(Ad\text{-}\kappa N9)(PTA)_2]$ [22], A further series of hydrogen bonds involving two disordered water molecules connect each neighbouring dimer through the atoms N2.

Complex **3** was obtained also from slow evaporation of its solution in H_2O as bright-yellow single crystals of the hydrated complex. The asymmetric unit contains a molecule of $[RuCp(Tf\text{-}\kappa N7)(mPTA)_2]^{2+}$ (Fig. 3), 1.5 water molecules and two disordered triflate anions. The most important distances and angles are summarized in Table 2. The molecular structure of the complex is constituted by a piano-stool cyclopentadienyl-ruthenium coordinated to two mPTA and a theophyllinate bonded by its nitrogen N7 (Ru1-N7 = 2.143(7) Å). As in **1**, the Ru—P bonds and the Ru-$Cp_{centroid}$ distances (Ru-$Cp_{centroid}$ = 1.856 Å; Ru-P1 = 2.258(2) Å; Ru-P2 = 2.269(2) Å) are slightly larger than in the starting complex $[RuCpCl(mPTA)_2](CF_3SO_3)_2$ (Ru-$Cp_{centroid}$ = Ru-P1 = 2.2509 (12) Å; Ru-P2 = 2.2599(12) Å). For what concern P—C and N—C distances in the mPTA ligand, they are practically the same found for **1** and similar complexes containing mPTA [24], The P-Ru-P angle is the

Table 2
Selected bond lengths and angles of **1** and **3**.

Bond lengths [Å] of **1**			Bond angles [°] of **1**			
Ru1	P1	2.2725(9)	P1	Ru1	P2	96.49(3)
Ru1	P2	2.2582(9)	N9	Ru1	P1	94.50(8)
Ru1	N9	2.117(3)	N9	Ru1	P2	93.80(8)
Ru1	$Cp_{centroid}$	1.857				
Bond lengths [Å] of **3**			Bond angles [°] of **3**			
Ru1	P1	2.258(2)	P1	Ru1	P2	96.24(8)
Ru1	P2	2.269(2)	N7	Ru1	P1	95.1(2)
Ru1	N7	2.143(7)	N7	Ru1	P2	92.18(19)
Ru1	$Cp_{centroid}$	1.856				

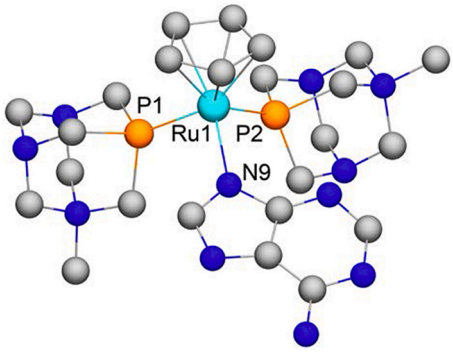

Fig. 1. Molecular structure of **1**. Hydrogen atoms, co-crystallized solvent and anions were omitted for clarity.

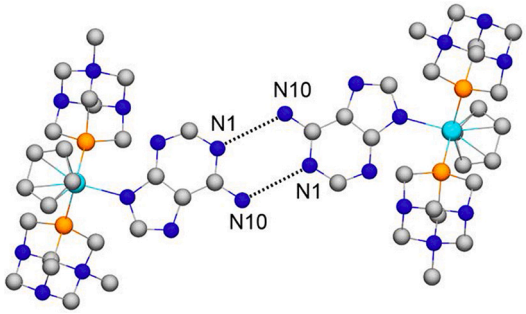

Fig. 2. Selected hydrogen bonds between two complex units of **1**. Hydrogen atoms, disorder components and anions were omitted for clarity.

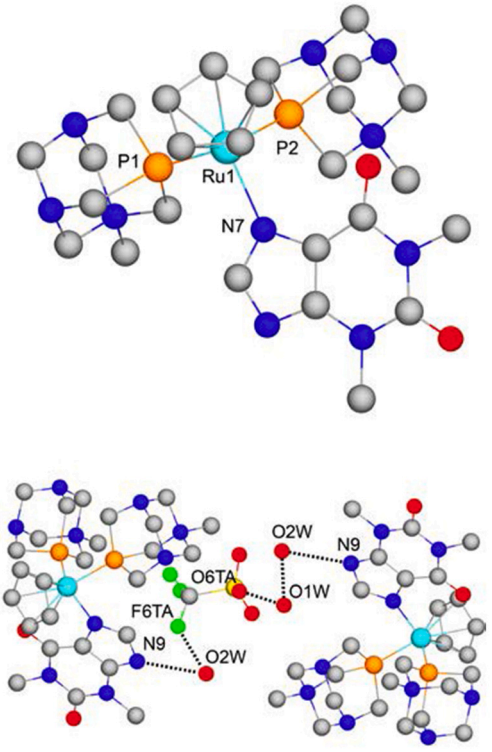

Fig. 3. Top: Molecular structure of **3**. Bottom: hydrogen bond network connecting the complex units. Hydrogen atoms and disorder components were omitted for clarity.

same to that in $[RuCpCl(mPTA)_2](CF_3SO_3)_2$ (P1-Ru-P2 = 96.19(9)° versus P1-Ru-P2 = 96.24(8)° in **3**). The complex units are connected through N9 with hydrogen bonds along the *a*-axis via the water molecules and the triflate anions (Fig. 3).

The adenine and theophyllinate ligands display similar imidazolic-ring bonds lengths: C8-N9 (**1**: 1.345(4) Å; **3**: 1.331(10) Å) and C8-N7 (**1**: 1.332(4) Å; **3**: 1.340(10) Å). This fact suggests that the bond character in both complexes is similar and intermediate between double and single, which contrasts with bond distances found in similar complexes containing adenine-κ*N9* and PTA ligands. In complexes [RuCp(Adeninate–κ*N9*)$(PTA)_2$] (C8-N9 = 1.363(4) Å; C8-N7 = 1.328(3) Å) and [RuCp(Adeninate–κ*N9*)(PPh_3)(PTA)] (C8-N9 = 1.328(3) Å; C8-N7 = 1.349(11) Å, the bond character of C8-N9 and C8-N7 are quite different [10], which is the expected setting for an adeninate anion coordinate to the ruthenium. Nevertheless the bond character is similar to those found in N7-N9 bridged Ru-adeninate complexes, such as complex $[\{RuCl(\mu_2\text{-adeninate-}N^7,N^9)(\eta^6\text{-p-cymene})\}_4]^{4+}$ (N9-C8 = 1.329(4) Å; C8-N7 = 1.335(4) Å) [25]. This fact supports the protonation of N7 as indicated by the refinement of the crystal structure [26–28]. Comparison of the C8-N7 and C8-N9 bond distances in **3** and the parent complex [RuCp(theophyllinate-κ*N7*)$(PTA)_2$] (C8-N7 = 1.339(6) Å; C8-N9 = 1.346(6) Å) indicates that these bonds have the same character in both complexes and other published theophyllinate complexes of Cu [29], Au [30], Cd [31], Hg [32,33], Co [34] and Zn [35].

3.3. Cell growth inhibition

The complexes **1**–**3** are soluble in water and polar solvents such as DMSO, but poorly soluble in organic solvents, being stable in solid-state and in solution under air at 40 °C for two days. In contrast, complexes **4**–**6** are poorly soluble in water but enough in DMSO for biological experiments, being also stable in solid-state and dissolution at 40 °C for two days under air. The six complexes have been tested for cell growth inhibition activity on human cancer cell lines *cis*platin-sensitive T2 and *cis*platin-resistant SKOV3. For comparison the complexes $[RuClCp(mPTA)_2](CF_3SO_3)_2$ and $[RuClCp(PPh_3)(mPTA)](CF_3SO_3)$ were also evaluated in the same panel of experiments. As a general procedure, each complex was dissolved in DMSO and diluted in AIM-V medium to obtain the final solutions with concentrations of 50, 10, and 2 μM respectively. The percentage of growth inhibition at the three doses for each complex provided the estimation of the concentration for reducing to 50% the cell growth of cell lines (IC50). The results obtained are summarized in Table 2 along with the solubility in water and the partition coefficient (Log *P*) of the complexes. Taking into account that the solubility and octanol-water partition coefficient are not so intertwined, a compound can be hydrophilic and yet soluble in organic solvents. The complexes **1**–**3** possess log *P* between 0 and − 0.7, and therefore the concentration of the compounds between the two phases is not even one order of magnitude different. Therefore, the fact that theses complexes display a poor antiproliferative activity in comparison to that for cisplatin cannot be directly correlated with their Log *P*. Nevertheless, it is reasonable to suppose that the scarce of solubility in organic solvents is an impediment for these complexes to cross the cytoplasmic membrane (Table 3).

In contrast, the complexes **4**–**6**, which contain one mPTA and one PPh_3, display a quite good antiproliferative activity in both cell lines, being significantly better versus the cisplatin-resistant cell SKOV3 line. Among similar complexes containing PTA and PPh_3 [22], the best antiproliferative activity was found for [RuCp(Adeninate–κ*N9*)(PPh_3)(PTA)] (<2 μM (T2); 30 ± 20 μM (SKOV3); Log *P* = 1.4; $S_{25,H2O}$ = 0.6; E_a = 0.690 mV) while for complexes with mPTA and PPh_3 the best activity was found for **5** (2–10 μM (T2); 2–10 μM (SKOV3); Log *P* = 0.35; $S_{25,H2O}$ = 1.4; E_a = 0.796 mV) but also the complexes **4** and **6** display a significant antiproliferative activity that is similar to that for cisplatin

Table 3
Estimated IC50 on *cis*platin sensitive T2 cell line and *cis*platin-resistant SKOV3 of complexes **1**–**6**, Log *P*, $S_{25,H2O}$ and E_o.

Complex	IC50 (μM)		Log *P*	$S_{25,H2O}$ (mg/cm^3)	E_o (mV)	Ref
	T2	SKOV3				
$[RuClCp(mPTA)_2](CF_3SO_3)_2$	> 50	> 50	−1.20		930	This work
[RuCp(Ad-κ*N9*)$(mPTA)_2](Cl_{0.5})(CF_3SO_3)_{2.5}$ (**1**)	>50	> 50	0.05	25.9	861	This work
[RuCp(Gu-κ*N9*)$(mPTA)_2](CF_3SO_3)_2$ (**2**)	> 50	> 50	−0.38	9.2	712	This work
[RuCp(Tf-κ*N7*)$(mPTA)_2](CF_3SO_3)_2$ (**3**)	>50	> 50	−0.69	16.1	737	This work
[RuClCp(PPh_3)(mPTA)](CF_3SO_3)	2–10	10–50	0.25	1.1	778	This work
[RuCp(Ad-κ*N9*)(PPh_3)(mPTA)](CF_3SO_3) (**4**)	2–10	10–50	0.40	1.3	837, 730	This work
[RuCp(Gu-κ*N9*)(PPh_3)(mPTA)](CF_3SO_3) (**5**)	2–10	2–10	0.35	1.4	796	This work
[RuCp(Tf-κ*N7*)(PPh_3)(mPTA)](CF_3SO_3) (**6**)	2–10	10–50	0.21	1.7	710	This work
*cis*platin	2–10	> 50				This work
$[RuClCp(PTA)_2]$	> 50	> 50	−1.85			[22]
[RuCp(Adeninate-κ*N9*)$(PTA)_2$]	>50	> 50	−0.82	15.8	620	[22]
RuCp(Guaninate-κ*N7*)$(PTA)_2$]	> 50	> 50	−1.19	3.5	974	[22]
[RuCp(Theophyllinate-κ*N7*)$(PTA)_2$]	>50	> 50	−0.45	14.0	684	[22]
[RuClCp(PPh_3)(PTA)]	10–50	> 50	0.75			[22]
[RuCp(Adeninate-κ*N9*)(PPh_3)(PTA)]	<2	10–50	1.40	0.6	690	[22]
[RuCp(Guaninate-κ*N7*)(PPh_3)(PTA)]	>50	> 50	1.32	0.4	407	[22]
[RuCp(Theophyllinate-κ*N7*)(PPh_3)(PTA)]	ca 50	ca 50	0.81	0.8	726	[22]

4. Conclusion

Six new complexes with general formula $[RuCp(Pur)LL']^{n+}$ (Pur = adenine (**1**), guaninate (**2**), theophyllinate (**3**); L = L' = mPTA. Pur = adeninate (**4**), guaninate (**5**), theophyllinate (**6**); L = mPTA, L' = PPh_3) were synthesized and characterized. The crystal structure of **1·H$_2$O** and **3·1.5H$_2$O** were determined by single-crystal X-ray diffraction. The antiproliferative activities of all the complexes were evaluated against cisplatin-sensitive T2 and cisplatin-resistant SKOV3 cell lines. Complexes **1**–**3** have not displayed antiproliferative activity in contrast with the complexes **4**–**6** that showed a slightly better antiproliferative activity than the neutral complexes [RuCp(*Pur*)LL'] (Pur = adeninate, guaninate, theophyllinate; L = PTA; L' = PTA, PPh_3), the starting complexes $[RuClCpLL']^{n+}$ and cisplatin. The complex **5**, containing mPTA, PPh_3 and guaninate, was found to be the most active in both cell lines (2–10 μM (T2); 2–10 μM (SKOV3); Log *P* = 0.35; $S_{25,H2O}$ = 1.4; E_a = 0.796 mV), being better than the cisplatin particularly on the SKOV3, which is resistant to the cisplatin. The complexes with mPTA are more hydrophilic than those with PTA, which favour their solubility in water and therefore in physiologic fluids. Complexes containing both mPTA and PPh_3 were those with larger antiproliferative activity. These complexes are enough soluble in water to achieve the needed concentration to act against the cancer cells but also are soluble in lipophilic systems such as the cell membranes, passing into the cell where they can act on the intracellular components such as DNA. On the other hand, the presence

of triphenylphosphine increases the hydro−/lipophilic balance. The substitution of the Cl^- in the starting complexes by a purine contributes also to obtain complexes with increased antiproliferative activity, which could be due to the interaction of the purines with the DNA bases by hydrogen bonds similar to those observed between the complex purine in the solid-state. This suspicion could be supported by the fact that among presented complexes those containing DNA-purines adenine and guanine display a better antiproliferative activity than theophylline, but more experiment should be done to ensure it. All the complexes display similar redox properties; therefore, this factor is not responsible for the observed cytotoxicity. The overall picture suggests that the best antiproliferative activity is rached when there is an adequate hydro−/lipophilic balance along with a possible contribution of complex-purine interactions with the pyrimidines of the nucleic acids. Nevertheless, more complexes should be synthesized and deeper studies must be done to confirm all these assumptions.

Declaration of Competing Interest

None.

Acknowledgements

Tanks are given the European Commission FEDER program for co-financing the projects CTQ2015-67384-R (MINECO), the Junta de Andalucía PAI-research group FQM-317. Thanks, are also given to A. Canella and P. Bergamini (U. Ferrara) for help with antiproliferative studies.

References

[1] B. Rosenberg, L. Van Camp, T. Krigas, Inhibition of cell division in Escherichia coli by electrolysis products from a platinum electrode, Nature. 205 (1965) 698–699, https://doi.org/10.1038/205698a0.
[2] E.R. Jamieson, S.J. Lippard, Structure, recognition, and processing of cisplatin-DNA adducts, Chem. Rev. 99 (1999) 2467–2498, https://doi.org/10.1021/cr980421n.
[3] B. Stordal, M. Davey, Understanding cisplatin resistance using cellular models, IUBMB Life 59 (2007) 696–699, https://doi.org/10.1080/15216540701636287.
[4] N. Pabla, Z. Dong, Cisplatin nephrotoxicity: mechanisms and renoprotective strategies, Kidney Int. 73 (2008) 994–1007, https://doi.org/10.1038/sj.ki.5002786.
[5] S. Medici, M. Peana, V.M. Nurchi, J.I. Lachowicz, G. Crisponi, M.A. Zoroddu, Noble metals in medicine: latest advances, Coord. Chem. Rev. 284 (2015) 329–350, https://doi.org/10.1016/j.ccr.2014.08.002.
[6] S. Betanzos-Lara, L. Salassa, A. Habtemariam, P.J. Sadler, Photocontrolled nucleobase binding to an organometallic RuII arene complex, Chem. Commun. (2009) 6622–6624, https://doi.org/10.1039/b914153g.
[7] J. Liu, H. Lai, Z. Xiong, B. Chen, T. Chen, Functionalization and cancer-targeting design of ruthenium complexes for precise cancer therapy, Chem. Commun. 55 (2019) 9904–9914, https://doi.org/10.1039/c9cc04098f.
[8] L. Zeng, P. Gupta, Y. Chen, E. Wang, L. Ji, H. Chao, Z.S. Chen, The development of anticancer ruthenium(II) complexes: from single molecule compounds to nanomaterials, Chem. Soc. Rev. 46 (2017) 5771–5804, https://doi.org/10.1039/c7cs00195a.
[9] A. Romerosa, P. Bergamini, V. Bertolasi, A. Canella, M. Cattabriga, R. Gavioli, S. Mañas, N. Mantovani, L. Pellacani, Biologically active platinum complexes containing 8-Thiotheophylline and 8-(Methylthio)theophylline, Inorg. Chem. 43 (2004) 905–913, https://doi.org/10.1021/ic034868c.
[10] P. Bergamini, V. Bertolasi, L. Marvelli, A. Canella, R. Gavioli, N. Mantovani, S. Mañas, A. Romerosa, Phosphinic platinum complexes with 8-thiotheophylline derivatives: synthesis, characterization, and antiproliferative activity, Inorg. Chem. 46 (2007) 4267–4276, https://doi.org/10.1021/ic062133c.
[11] A. Romerosa, T. Campos-Malpartida, C. Lidrissi, M. Saoud, M. Serrano-Ruiz, M. Peruzzini, J.A. Garrido-Cárdenas, F. García-Maroto, Synthesis, characterization, and DNA binding of new water-soluble cyclopentadienyl ruthenium(II) complexes incorporating phosphines, Inorg. Chem. 45 (2006) 1289–1298, https://doi.org/10.1021/ic051053q.
[12] L. Hajji, C. Saraiba-Bello, A. Romerosa, G. Segovia-Torrente, M. Serrano-Ruiz, P. Bergamini, A. Canella, Water-soluble Cp ruthenium complex containing 1,3,5-triaza-7-phosphaadamantane and 8-thiotheophylline derivatives: synthesis, characterization, and antiproliferative activity, Inorg. Chem. 50 (2011) 873–882, https://doi.org/10.1021/ic101466u.
[13] W.L.F. Armarego, C. Chai, Purification of Laboratory Chemicals, Elsevier Inc., 2009, https://doi.org/10.1016/C2009-0-26589-5.
[14] J. Volhard, Ueber eine neue Methode der maassanalytischen Bestimmung des Silbers, J. Für Prakt. Chemie. 9 (1874) 217–224, https://doi.org/10.1002/prac.18740090117.
[15] O.V. Dolomanov, L.J. Bourhis, R.J. Gildea, J.A.K. Howard, H. Puschmann, OLEX2: a complete structure solution, refinement and analysis program, J. Appl. Crystallogr. 42 (2009) 339–341, https://doi.org/10.1107/S0021889808042726.
[16] G.M. Sheldrick, SHELXT - integrated space-group and crystal-structure determination, Acta Crystallogr. Sect. A Found. Crystallogr. 71 (2015) 3–8, https://doi.org/10.1107/S2053273314026370.
[17] G.M. Sheldrick, Crystal structure refinement with SHELXL, Acta Crystallogr. Sect. C Struct. Chem. 71 (2015) 3–8, https://doi.org/10.1107/S2053229614024218.
[18] M.B. Hansen, S.E. Nielsen, K. Berg, Re-examination and further development of a precise and rapid dye method for measuring cell growth/cell kill, J. Immunol. Methods 119 (1989) 203–210, https://doi.org/10.1016/0022-1759(89)90397-9.
[19] R. Mannhold, G.I. Poda, C. Ostermann, I.V. Tetko, Calculation of molecular lipophilicity: state-of-the-art and comparison of log P methods on more than 96000 compounds, J. Pharm. Sci. 98 (2009) 861–893, https://doi.org/10.1002/jps.21494.
[20] H.R. Lozano, F. Martínez, Thermodynamics of partitioning and solvation of ketoprofen in some organic solvent/buffer and liposome systems, Rev. Bras. Ciencias Farm. J. Pharm. Sci. 42 (2006) 601–613, https://doi.org/10.1590/S1516-93322006000400016.
[21] L. Ropel, L.S. Belvèze, S.N.V.K. Aki, M.A. Stadtherr, J.F. Brennecke, Octanol-water partition coefficients of imidazolium-based ionic liquids, Green Chem. 7 (2005) 83–90, https://doi.org/10.1039/b410891d.
[22] L. Hajji, C. Saraiba-Bello, G. Segovia-Torrente, F. Scalambra, A. Romerosa, CpRu complexes containing water soluble Phosphane PTA and natural purines adenine, guanine and theophylline: synthesis, characterization, and Antiproliferative properties, Eur. J. Inorg. Chem. (2019) 4078–4086, https://doi.org/10.1002/ejic.201900677.
[23] The Cambridge Crystallographic Data Centre (CCDC). https://www.ccdc.cam.ac.uk/, 2021 (accessed June 6, 2020).
[24] L. Hajii, C. Saraiba Bello, F. Scalambra, G. Segovia-Torrente, A. Romerosa, A. Canella, Ruthenium complexes containing mPTA and thiopurines bis(8-thiotheophylline)-$(CH_2)_n$ (n = 1–3; mPTA = N-methyl-1,3,5-triaza-7-phosphaadamantane), J. Coord. Chem. 70 (2017), https://doi.org/10.1080/00958972.2017.1311411.
[25] K. Krogh-Jespersen, R.T. Stibrany, E. John, J.D. Westbrook, T.J. Emge, M.J. Clarke, J.A. Potenza, H.J. Schugar, Solid-state changes in ligand-to-metal charge-transfer spectra of $(NH_3)_5Ru^{III}$ (2,4-dihydroxybenzoate) and $(NH_3)_5Ru^{III}$ (xanthine) chromophores, Inorg. Chem. 47 (2008) 9813–9827, https://doi.org/10.1021/ic800511g.
[26] W.S. Sheldrick, C. Landgrafe, Di- and trinuclear (η^6-arene)ruthenium(II) complexes containing bridging heterocyclic thioamides, Inorganica Chim. Acta. 208 (1993) 145–151, https://doi.org/10.1016/S0020-1693(00)85114-2.
[27] S. Korn, W.S. Sheldrick, Oligomeric (η^6-arene) ruthenium(II) complexes of adenine and adenosine with N6,N7 coordination, Inorganica Chim. Acta. 254 (1997) 85–91, https://doi.org/10.1016/S0020-1693(96)05146-8.
[28] S. Korn, W.S. Sheldrick, pH-Dependent competition between κ^2N7,O(P) macrochelation and μ-N1,N7 oligomer formation for (η^6-arene)Ru(II) complexes of adenosine and guanosine 5′-mono-, −di- and -tri-phosphates, J. Chem. Soc. Dalt. Trans. (1997) 2191–2200, https://doi.org/10.1039/a700976c.
[29] T.J. Kistenmacher, D.J. Szalda, L.G. Marzilli, Intercalative Stacking Interactions and Interligand Hydrogen Bonding in Metal Purine Complexes. Crystal and Molecular Structure of (N-Salicylidene-N'-methylethylenediamine) (theophyllinato)copper(II) Monohydrate, Inorg. Chem. 14 (1975) 1686–1691, https://doi.org/10.1021/ic50149a051.
[30] E. Colacio, A. Romerosa, J. Ruiz, P. Román, J.M. Gutiérrez-Zorrilla, M. Martínez-Ripoll, Reactions of chloro(triphenylphosphine)gold(I) and [μ-l,2-bis (diphenylphosphine)ethane]-bis[bromogold(I)] with oxopurine bases. Molecular and crystal structure and bonding of (theophyllinato)(triphenylphosphine)gold(I), J. Chem. Soc., Dalt. Trans. (1989) 2323–2329, https://doi.org/10.1039/DT9890002323.
[31] E. Buncel, R. Kumar, A.R. Norris, A.L. Beauchamp, Metal ion biomolecule interactions. PART VII. Synthesis, spectroscopic properties and crystal structure investigations of some bis(theophyllinato)tetraaquocadmium(II) compounds, Can. J. Chem. 63 (2006) 2575–2581, https://doi.org/10.1139/v85-427.
[32] A.A. Norris, S.E. Taylor, E. Buncel, F. Bélanger-Gariépy, A.L. Beauchamp, Crystal structure of (theophyllinato)methylmercury(II) monohydrate, Inorganica Chim. Acta. 92 (1984) 271–274, https://doi.org/10.1016/S0020-1693(00)80049-3.
[33] K. Caldwell, G.B. Deacon, B.M. Gatehouse, S.C. Lee, A.J. Canty, Organomercury medicinal chemistry. Synthesis and structure of a (β-methoxyethyl)mercury(II) derivative of N(7)-deprotonated theophylline, $[Hg(C_3H_7O)(C_7H_7N_4O_2)]$, Acta Crystallogr. Sect. C Cryst. Struct. Commun. 40 (2002) 1533–1536, https://doi.org/10.1107/s010827018400860x.
[34] T.J. Kistenmacher, trans-[Theophyllinatochlorobis(ethylenediamine) cobalt(III)] chloride dihydrate, Acta Crystallogr. Sect. B Struct. Crystallogr. Cryst. Chem. 31 (2002) 85–89, https://doi.org/10.1107/s0567740875002142.
[35] M.J. Gardner, R.X. Smith, E. Shefter, Zn(II)–theophylline–Ethylenediamine: structure and pH stability, J. Pharm. Sci. 72 (1983) 348–350, https://doi.org/10.1002/jps.2600720407.